Novel fabrication tools for dynamic compression targets with engineered voids using photolithography methods **EP**

ⓘ Silvia Pandolfi, ⓘ Thomas Carver, Daniel Hodge, et al.

COLLECTIONS

EP   This paper was selected as an Editor's Pick

View Online   Export Citation   CrossMark

ARTICLES YOU MAY BE INTERESTED IN

A comprehensive review and outlook on the experimental techniques to investigate the complex dynamics of pulsed laser ablation in liquid for nanoparticle synthesis
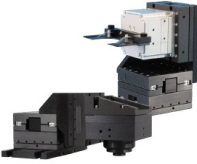Review of Scientific Instruments **93**, 091501 (2022); https://doi.org/10.1063/5.0084803
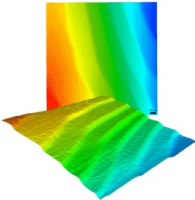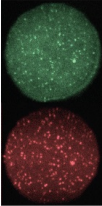
A new μ−high energy resolution fluorescence detection microprobe imaging spectrometer at the Stanford Synchrotron Radiation Lightsource beamline 6-2
Review of Scientific Instruments **93**, 083101 (2022); https://doi.org/10.1063/5.0095229

Sub-millinewton thrust stand and wireless power coupler for microwave-powered small satellite thrusters
Review of Scientific Instruments **93**, 083507 (2022); https://doi.org/10.1063/5.0088831

AIP Publishing

Novel fabrication tools for dynamic compression targets with engineered voids using photolithography methods

View Online   Export Citation   CrossMark

Silvia Pandolfi,[1,a] Thomas Carver,[2] Daniel Hodge,[3] Andrew F. T. Leong,[4] Kelin Kurzer-Ogul,[5] Philip Hart,[1]
Eric Galtier,[1] Dimitri Khaghani,[1] Eric Cunningham,[1] Bob Nagler,[1] Hae Ja Lee,[1] Cindy Bolme,[4]
Kyle Ramos,[4] Kenan Li,[1] Yanwei Liu,[1] Anne Sakdinawat,[1] Stefano Marchesini,[1] Pawel M. Kozlowski,[4]
Chandra B. Curry,[1,6] Franz-Joseph Decker,[1] Sharon Vetter,[1] Jessica Shang,[5,7] Hussein Aluie,[5,7]
Matthew Dayton,[8] David S. Montgomery,[4] Richard L. Sandberg,[3] and Arianna E. Gleason[1]

AFFILIATIONS

[1] SLAC National Accelerator Laboratory, 2575 Sand Hill Rd., Menlo Park, California 94025, USA
[2] Stanford Nano Shared Facilities, Stanford University, Palo Alto, California 94305, USA
[3] Department of Physics and Astronomy, Brigham Young University, Provo, Utah 84602, USA
[4] Los Alamos National Laboratory, Los Alamos, New Mexico 87545, USA
[5] Department of Mechanical Engineering, University of Rochester, Rochester, New York 14623, USA
[6] Department of Electrical and Computer Engineering, University of Alberta, Edmonton, Alberta T6G 1H9, Canada
[7] Laboratory for Laser Energetics, University of Rochester, Rochester, New York 14623, USA
[8] Advanced hCMOS Systems, 6300 Riverside Plaza Ln. Suite 100, Albuquerque, New Mexico 87107, USA

[a] Author to whom correspondence should be addressed: silviap@stanford.edu

ABSTRACT

Mesoscale imperfections, such as pores and voids, can strongly modify the properties and the mechanical response of materials under extreme conditions. Tracking the material response and microstructure evolution during void collapse is crucial for understanding its performance. In particular, imperfections in the ablator materials, such as voids, can limit the efficiency of the fusion reaction and ultimately hinder ignition. To characterize how voids influence the response of materials during dynamic loading and seed hydrodynamic instabilities, we have developed a tailored fabrication procedure for designer targets with voids at specific locations. Our procedure uses SU-8 as a proxy for the ablator materials and hollow silica microspheres as a proxy for voids and pores. By using photolithography to design the targets' geometry, we demonstrate precise and highly reproducible placement of a single void within the sample, which is key for a detailed understanding of its behavior under shock compression. This fabrication technique will benefit high-repetition rate experiments at x-ray and laser facilities. Insight from shock compression experiments will provide benchmarks for the next generation of microphysics modeling.

Published under an exclusive license by AIP Publishing. https://doi.org/10.1063/5.0107542

I. INTRODUCTION

Mesoscale imperfections and inhomogeneities in structure and composition play a crucial role in the physical and chemical behavior of all materials. The mechanical properties and response of materials, especially at extreme conditions, e.g., at pressures above a Mbar, are largely dictated by the microstructure and defect content.

Material defects can be planar at domain interfaces or grain boundaries, linear like dislocations, or a single point or location in a structure, such as chemical impurities or vacancies. An accumulation of defects or vacancies in any material can lead to void or pore space formation. The need to understand how voids and the void collapse process dictate materials performance under extreme conditions intersects many materials science applications and a range

of disciplines, such as geophysics,[1] and planetary- and fusion energy sciences.[2,3]

Characterizing the response of void defects and void collapse during dynamic compression is critical for predicting the microphysics dictating the material's response as the collapse process can seed hydrodynamic instabilities.[4–9] One area of study where the material properties and the seeding of instabilities are particularly problematic is Inertial Confinement Fusion (ICF) physics.[10] Here, a uniform spherical implosion of fuel inside a capsule is necessary to generate thermonuclear ignition;[11,12] potentially, ignition could open an exciting area of research for future global clean energy solutions, termed Inertial Fusion Energy (IFE).[13–16] However, the presence of defects, particularly voids, in the ablator layer, i.e., the outermost material of the capsule, has been recognized as one of the major contributions to performance degradation due to instability seeding and growth.[17] Micron-sized voids and pores in the ablator layer have been suggested to possibly cause jetting as the collapse process generates ejecta with roughly double the particle velocity of the bulk material, launching Rayleigh–Taylor hydrodynamic instabilities,[18–20] which limits compression of the fuel and fusion performance. A precise understanding of the response of mesoscale defects, such as voids, in the ablator material, is thus key for advancing ICF and IFE.

New experimental benchmark data are required to refine current microphysics models of void collapse under shock compression, which include a combination of material strength, radiation transport, instability tracking, equation of state, and transport properties.[21] To specifically tackle an understanding of how voids dictate a material's response to dynamic compression, a well-characterized void feature is needed. To do this, we developed a fabrication procedure to enable the design and characterization of a simplified system, i.e., an isolated void and its interaction with the propagating shock wave and the surrounding material. Dynamic compression is achieved by focusing a high-power laser onto the sample to generate ablation-driven shock compression (Fig. 1, right panel). As shown in Fig. 1, specific placement of the void within the sample is required by the experimental geometry. To ensure homogeneous spatial compression, the void needs to be centered with respect to the drive surface, i.e., the xy-plane in Fig. 1. Furthermore, the distance between the void and the drive surface (d along the z-axis in Fig. 1) should be tunable.

Future x-ray free electron laser (XFEL) experiments, with the expected upgrades of optical driver lasers to 1 Hz frequency, will be conducted at high-repetition rates and will require large-scale target production[22] (i.e., one sample and one compression every second, compared to the current shot cycle of 5–7 min). To satisfy these requirements, there is an ongoing effort in the community to develop new strategies for mass scale production of samples. Recently, Smith *et al.* have demonstrated a novel fabrication procedure for slurry targets that use particles embedded in epoxy to produce "ribbons" of materials.[22] Here, we present the photolithography-based fabrication of targets for dynamic compression containing isolated voids. This method allows for large-scale production of individual designer targets with tuned microstructures and properties, which is a key requirement for the study of mesoscale imperfections under dynamic compression. The precise and reproducible placement of an isolated void within the sample is viable with this methodology; the study of such simplified systems will provide precise and detailed insight into the behavior of micrometer-sized voids under dynamic compression. This fabrication method can also be extended to other fields of high-energy density science, e.g., viscosity measurements that use isolated heterogeneities embedded in the bulk.[23–25] Large-scale, designer target fabrication procedures will also be key in the development of the IFE industry, where 10 Hz rep-rated laser technology could drive the foundational design of future fusion power plants.[26]

II. METHOD

A. Materials

Polystyrene $(C_8H_8)_n$ and other plastic materials, e.g., glow deposition polymer,[27–30] are commonly used as ablator materials in ICF experiments. Here, to investigate their properties and the interaction of defects with a propagating shock wave, we have used the photoresist SU-8[31] as a proxy. SU-8, made by Kayaku Advanced Materials, is a mixture of photosensitive epoxy resin, epoxy novolac polymer, and various solvents. The mixture is a viscous liquid that can be easily deposited and spun into layers. That is to say, SU-8 can be deposited onto a substrate, and, by fast rotation, the SU-8 solution is distributed via centrifugal force, resulting in a homogeneous coverage, while the excess material is ejected; several layers of SU-8 can be spun on top of each other before exposure and hardening.[32] The solvents and their proportions can be manipulated to achieve different viscosities, which can produce layers with thicknesses ranging from 0.5 to >200 μm. The vendor provides calibrated spinning protocols, indicating the approximate thickness that can be obtained depending on spinning speed, duration, and the viscosity of the starting SU-8 material. The SU-8 epoxy cross-links and hardens
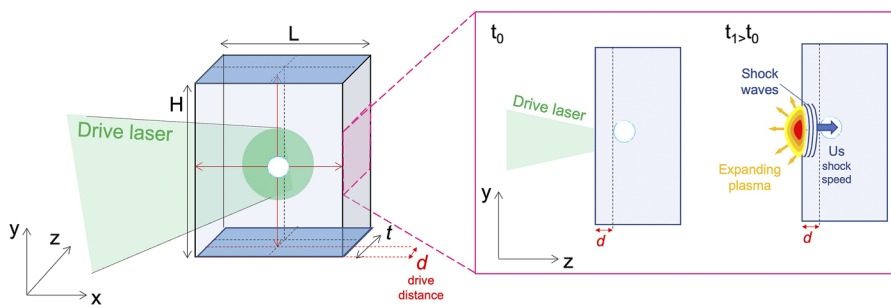

FIG. 1. Left: schematic view of ideal sample for void collapse; the compression is driven by a high-power laser focused on the sample's drive surface ($x–y$ plane). The inset on the right shows the working principle of laser-driven shock-compression: the formation of an expanding plasma at the drive surface generates shock waves that compress the sample along the laser propagation direction (z).

when exposed to ultraviolet light (optimal wavelength 365 nm), and the unexposed parts can be dissolved.[33] By using appropriate photolithography masks, this allows for the production of geometries with high precision.

The experimental requirements for these targets are multifaceted—not only do they need to be similar in properties and shock response to traditional polymer ICF ablators but they also need to have a uniform thickness for dynamic x-ray imaging measurements and be uniform laterally for steady shock propagation. SU-8 has a similar density (1.2 g/cm^3),[34] mechanical (Young's modulus 4.1 GPa),[35] and optical (refractive index 1.6)[36] properties as polystyrene.[37] The practical advantages when using SU-8 as a proxy for other polymers is that being a photoresist, it can be spun over a substrate to obtain a homogeneous layer. Moreover, photolithography enables the production of devices with specific geometries and a resolution on the order of a few micrometers. The final result is an optically transparent device whose thickness can be specified by spinning various formulations of SU-8 of the appropriate viscosity (commercially available) and tuning the spinning speed and duration. In particular, for our study, the quality of the lateral walls is crucial, and SU-8 enables control and fabrication of nearly vertical sidewalls, even in devices with very high aspect ratios:[38–40] this will ensure the planarity of the driven shock as well as the ability to use a suite of characterizations, e.g., velocimetry for pressure measurements[41] or x-ray based imaging techniques.[42–46]

In our fabrication procedure, we used hollow silica glass shells as a proxy for the actual voids. Such hollow glass shells are commercially available (Cospheric LLC) as microspheres made of a proprietary soda-lime borosilicate formulation with nominal wall thicknesses up to a few μm. Hollow microspheres with metallic coatings are also available, which can be used to tune their mechanical as well as conductive properties. Due to the small thickness of the microsphere silica shell (estimates ~1.5 μm), the behavior

of our devices under shock-compression is consistent with that of a device containing an actual void of the same size, as shown in Fig. 2. Hydrodynamic simulations show similar flows and polymer density for the shock-compression of a 40 μm void and a 40 μm silica shell with 2 μm-thick walls, demonstrating that the hollow microsphere behavior can provide significant insight into the physics of void collapse. There are numerous advantages in using silica microspheres over other void-fabrication techniques like laser milling: (i) versatility, as the microspheres are available in a wide range of sizes 5–125 μm; (ii) cost reduction, as the microspheres can be purchased in large quantities and are relatively inexpensive; (iii) time-saving, as, for each SU-8 spinning, numerous void-bearing devices can be produced, as opposed to the time required to prepare the bare devices and individually laser-mill the desired void for each device. Furthermore, the ability to produce many samples with a single spinning procedure also ensures high homogeneity within each batch. The effectiveness and scalability of this fabrication approach procedure make it suitable for the next generation of ICF and high-energy density XFEL-based experiments, as it can meet the increased need for targets once high repetition rate driver lasers are available.

B. Experimental procedure

The ideal target design for ICF void-bearing ablators is shown in Fig. 3. As previously mentioned, the void should be centered in the laser drive surface (xy-plane) and placed at a specific distance d from the drive surface (i.e., along the z-axis). Specifically, for our experiments, we used ~40 μm hollow silica microspheres (HSG 38-45ect), and the desired d value was ~30 μm. However, the size of the microsphere as well as the device's dimensions can easily be tuned using this fabrication procedure. We developed our fabrication procedure at the Stanford Nano Shared Facilities (SNSF) at Stanford University, CA (USA). SU-8 was spun onto a substrate using a
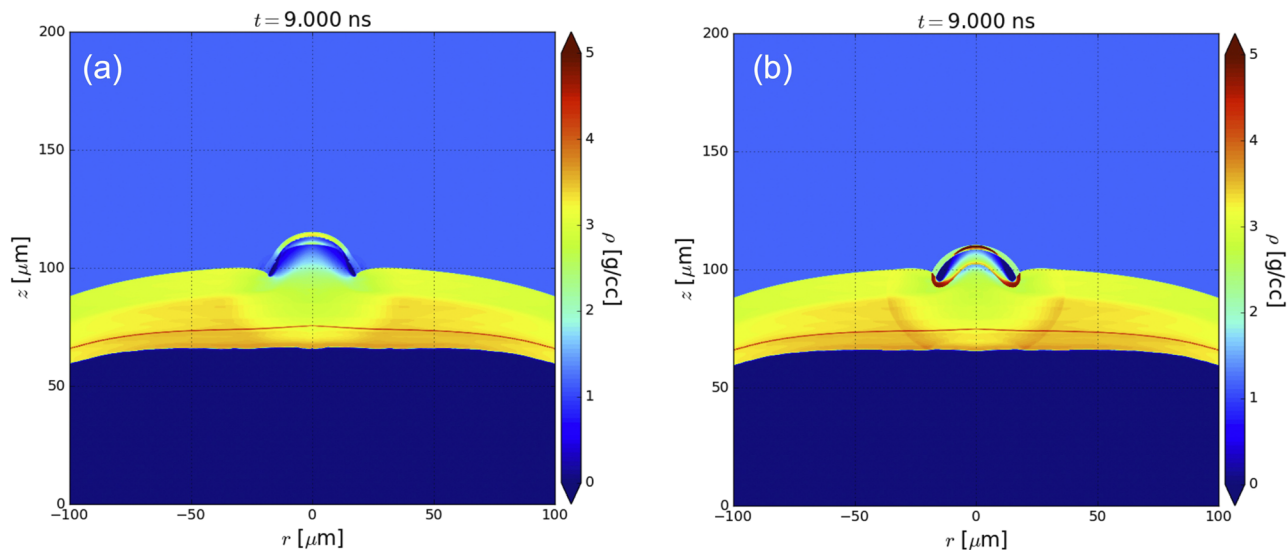

FIG. 2. Hydrodynamic simulations of shock-compressed SU-8 embedding: (a) a 40 μm spherical void and (b) a 40 μm hollow SiO$_2$ shell with 2 μm-thick walls.

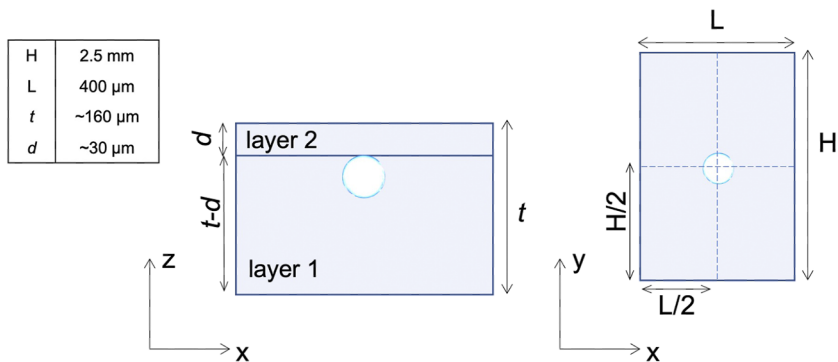| H | 2.5 mm |
L	400 μm
t	~160 μm
d	~30 μm

FIG. 3. Schematic view of ideal sample geometry for x-ray imaging experiment under shock compression.

Headway PWM32-PS-CB15 spinner; several layers can be superposed before exposure, allowing to build up stratified devices of the desired thickness t. For our experiments, we used a 3 in. silicon wafer as a substrate and spun different metal layers over it (i.e., 50 nm of the copper adhesion layer and titanium coating) to increase the adhesion and thickness uniformity of the photoresist during spinning. The microspheres were heated at 150 °C for about 15–20 min to dry out adsorbed moisture on the surfaces and separate beads that were clumped together, allowing them to fall individually.

From preliminary tests with the 40 μm microspheres, we have noticed full wetting of the beads after dispersion onto an unexposed SU-8 layer, so we designed the target fabrication as follows: For a device of desired thickness t and bead-drive distance d (see Figs. 1 and 2): (i) spin a layer of SU-8 of thickness $t-d$; (ii) deposit the bead, either by sprinkling them or by singularly placing them onto the substrate; (iii) spin an additional layer of SU-8 of thickness d. In this way, the microspheres are fully wetted by layer 1 and sink to the level, so d can be directly tuned by changing the spinning parameters of layer 2. The parameters from our optimized fabrication procedure are reported in Table I. We have used the SU-8 2050 solution as starting material for both layers. Even though, nominally, the final SU-8 density should not depend on the viscosity of the starting material, using only one solution throughout the whole fabrication ensured to obtain a more homogeneous device, avoiding eventual microstructural or density inhomogeneities.

Within the SNSF, a Durham Magneto Optics ML3 MicroWriter direct write (maskless) exposure machine operating at 385 nm was available. Despite 385 nm not being the optimal wavelength to cross-link SU-8, the photoresist could still be successfully processed by increasing the exposure dose to achieve full hardening (Fig. 4). Further experimentation with dose and defocus helped to enhance the sidewall geometry to make optically smooth, nearly vertical sidewalls. With respect to our procedure, the exposure dose and processing time can be reduced by using the most suited 365 nm UV wavelength. We used the microscope of the direct write machine to examine the substrate and the SU-8 and to locate the beads. The center of the beads is easily detected, as the spheres exhibit a bright reflection from their exact center; we used this bright reflection to determine their coordinates in X and Y with ~1 μm accuracy. For exposure and cross-link, a rectangular mask of the desired dimensions (in our case 400 μm × 2.5 mm) was designed and centered in X and Y, which ensured the precise placement of the bead in the xy-plane of the device (Fig. 3, right panel). The machine can be set up to expose the rectangular patterns sequentially on the microsphere's coordinates, allowing for the production of several devices for each exposure; this approach can be readily expanded to different target and/or bead placement geometries by simply modifying the exposure mask design. By varying the exposure dose, different results in terms of SU-8 cross-link and edge sharpness can be obtained, as shown in Fig. 4. For example, 2000 mJ/cm² is not sufficient to fully expose the SU-8: the device appears opaque at the optical microscope, which suggests that the bottom layer is partially unexposed and thus does not exhibit the optical quality and transparency of fully cross-linked SU-8. No noticeable changes are observed varying the exposure dose between 2200 and 2600 mJ/cm², and the

TABLE I. Explanation of parameters.

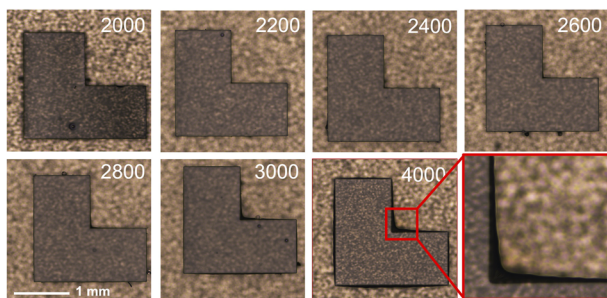| Layer	Thickness	Value (μm)	Spin speed (RPM)	Ramp (RPM/s)	Time (s)	Bake temp. (°C)	Bake time (min)
Layer 1	$t-d$	130	500 1500	100 300	10 30	65; 95	7; 40
Deposit hollow microspheres							
Layer 2	d	30	500 3300	100 300	10 30	95	5

FIG. 4. Example of exposure tests, in which the exposure dose was systematically changed; the numbers on each figure indicate the exposure dose for each device (expressed in mJ/cm^2).

devices appear transparent with sharp edges; for exposure doses of 2800 mJ/cm^2 and higher, the corner starts to look less sharp and darker at the optical microscope. The darker edges and corners indicate that the sidewalls of the devices are slightly tilted, with a larger cross-linked area toward the bottom of the device; this results from overexposure, as the bottom layer is crossed-linked not only from direct irradiation but also from non-perpendicular light reflected by the metallic coating on the substrate. While overexposure slightly affects the vertical sidewalls, it also ensures that the whole device, down to the substrate, is fully cross-linked. For our optimized fabrication procedure, we used a 10X microscope and lens setting with a nominal exposure resolution of 1 μm; we estimate our actual resolution to be of the order of 2–3 μm, as we slightly overexposed our devices to ensure complete cross-link of the epoxy and good mechanical properties under shock-compression (3000 mJ/cm^2, see Fig. 4). A slight over-exposure was preferred for this protocol to compensate eventual shadowing from the microsphere, as shown in Fig. 7 and discussed in Sec. III. It is worth noting that because the positions of the microspheres are individuated and recorded

manually one at a time, the uncertainty on the bead placement within the device depends solely on the microscope and the direct write machine resolutions, which is thus of the order of 2–3 μm, without being affected by the batch size.

After exposure, the spun SU-8 was baked at 65° for 5 min and then at 95° for 13 min. Subsequently, the whole wafer was submerged in SU-8 Developer (mfg. by Kayaku Materials) for 15 min and gently turned to dissolve all the non-exposed photoresists. After this step, only the exposed cross-linked region, i.e., the devices, remains on the substrate while the rest of the SU-8 is dissolved and rinsed away. After development and full cross-link, the SU-8 adhesion to the substrate decreases, and the devices can be mechanically detached from the substrate using a fine and anti-scratch tweezer for leverage. We have tested other extraction methods, such as dissolving a sacrificial layer of Al or Cu, but we have discovered that the metal etchants unexpectedly dissolve the SU-8 and/or compromise the optical quality of the devices' walls. However, the possibility of mechanically extracting the devices simplifies the procedure, as it does not require rinsing, filtering, and recovering the parts from the etchants.

Furthermore, we noted that using a metallic layer on top of the Si substrate facilitates mechanical extraction of the devices, which can be easily peeled off the wafer without damage. The final step for completing the curing and hardening of the extracted targets was a 10 min bake at 150 °C.

III. RESULTS

Following the procedure detailed in Sec. II, up to 50–60 void-bearing SU-8 devices can be fabricated from a single SU-8 processing, ensuring high homogeneity within each batch. After completing the fabrication, we used x-ray computed tomography (CT) to determine whether the procedure had affected the voids; the results are shown in Fig. 5. X-ray CT is a non-destructive scanning x-ray imaging technique that, by collecting angle-resolved x-ray images of the
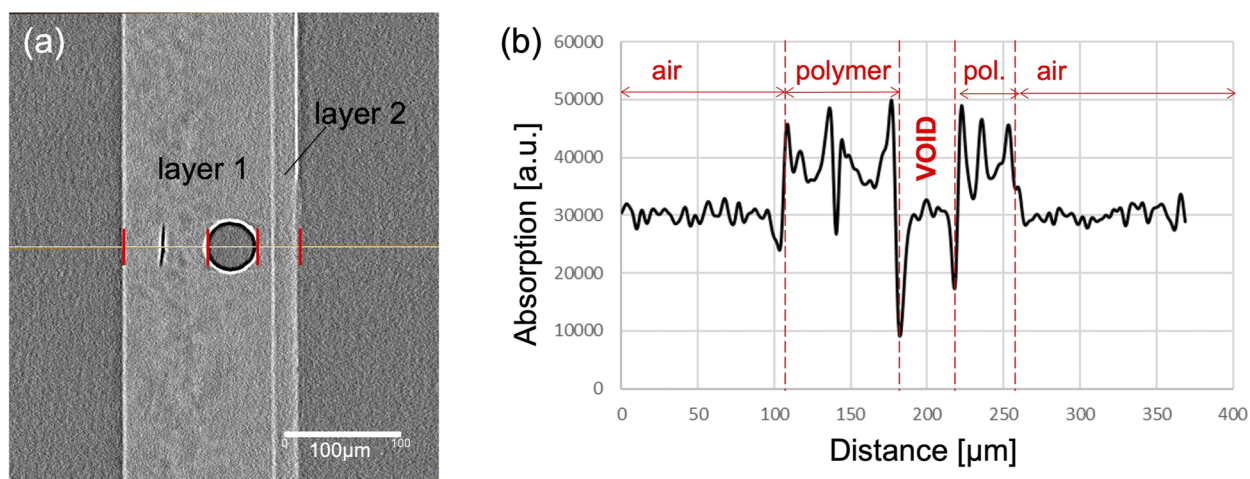

FIG. 5. X-ray CT measurements of a representative SU-8 void-bearing target (Carl Zeiss X-ray Microscopy, Inc. Xradia Versa 520). (a) 2D reconstructed slice at the void center. (b) X-ray absorption spectrum as measured along the yellow line in (a); the different parts and materials are indicated.
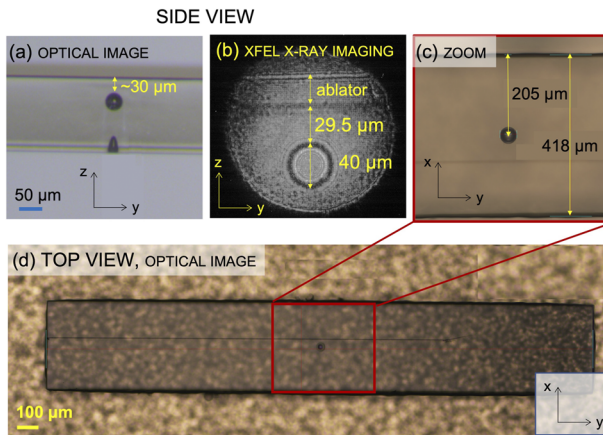
SIDE VIEW

(a) OPTICAL IMAGE ~30 μm, 50 μm

(b) XFEL X-RAY IMAGING — ablator, 29.5 μm, 40 μm

(c) ZOOM — 205 μm, 418 μm

(d) TOP VIEW, OPTICAL IMAGE — 100 μm

FIG. 6. Representative images of void-bearing SU-8 targets; both optical (a), (c), and (d) and x-ray (b) images confirm the production of targets with the desired geometry.

sample, can provide reconstructed 2D slices at specific depths within the sample.[47] Figure 5(a) shows the reconstructed slice at the center of the device; the microsphere size (~40 μm diameter) and the void depth d (~30 μm) are consistent with the expected values. Importantly, x-ray absorption was measured along the yellow line in Fig. 5(a). The results are reported in Fig. 5(b) and show that the region inside the void display the same x-ray absorption as the air surrounding the device, which confirms that no chemical or solvent penetrates the glass walls, and the microspheres remain empty throughout the whole fabrication procedure. Thus, the hollow silica microspheres embedded in cross-linked SU-8 following our experimental protocol are a suitable proxy for actual voids within the sample.

We performed further imaging characterization to confirm the microsphere placement within the device as well as checking the optical quality of the devices' lateral walls; the results are reported in Fig. 6. The optical image in Figs. 6(c) and 6(d) shows the "top view," which corresponds to the xy-plane in Figs. 1 and 2, i.e., the surface on which the driver laser is focused for laser-driven shock-compression. As previously mentioned, shock-compression experiments require the voids to be centered on this surface to ensure planar and homogeneous compression. Precise placement of the microsphere was successful using photolithography to cross-link the SU-8 in a region centered around an isolated microsphere (Sec. II B). We have also analyzed the placement of the void along the direction of the shock propagation, i.e., the z axis in Figs. 1 and 2. The optical image

reported in Fig. 6(a) shows that our results are consistent with the desired value of ~30 μm, thus the fabrication procedure allows us to accurately define this distance by optimizing the spinning conditions of the second SU-8 layer (Sec. II B). However, optical measurements through a transparent medium could be affected by aberrations, especially when looking at the "side view," as the images are collected through a 400 μm-thick layer of SU-8. For this reason, we have also used x-ray imaging techniques [x-ray CT in Fig. 5 and XFEL-based x-ray imaging in Fig. 6(b)] to confirm the value and the reproducibility of the desired void-drive distance d. Our fabrication procedure is thus suited for the design of devices embedding voids at specific locations, as shown in Fig. 6, and the results were highly reproducible over hundreds of devices. It is also worth noting that our ability to obtain clear images of the beads through 100 up to 400 μm of SU-8 demonstrates the high optical quality of the devices' lateral walls.

As detailed in Sec. II B, we have spun the thick layer incorporating the voids first, and then a second layer to ensure that the microspheres are at the desired depth d within the sample. Besides the advantage of an easily tunable procedure to optimize d, this choice was also dictated by the necessity to ensure full exposure through the total thickness of the device. Indeed, the microspheres dispersed in the SU-8 can cause shadowing during the photolithography process and affect the full cross-link of the region beneath them; results from our preliminary tests are reported in Fig. 7. As visible by the "side view" of these devices, having the microsphere on top of a thick layer [Fig. 7(a)] can mitigate the shadowing effects experienced by a microsphere placed closer to the wafer substrate [Fig. 7(b)]. It is probable, indeed, that having more space between the silica shell and the metallic substrate allows for more photons to be reflected from the metallic surface of the substrate. Thus, even if not by direct irradiation, the region beneath the microsphere is still exposed, and it cross-links. On the contrary, when the microsphere is too close to the bottom of the device, the shadowing effects dominate, and the region beneath it is not exposed such that the sphere sinks to the bottom, as shown in Fig. 7(b). This further emphasizes the importance of the slight overexposure of the device that we adopted. Indeed, not only it ensures cross-link of bare SU-8 but also full exposure beneath the microsphere, in the region shadowed from direct irradiation.

IV. SUMMARY

We have developed and tested a fabrication procedure that allows for large-scale production of void-bearing targets for dynamic compression experiments. We used SU-8 photoresist and hollow silica microspheres as proxies for void-bearing ICF ablator materials. Our fabrication procedure exploits the spinning of SU-8 layers at
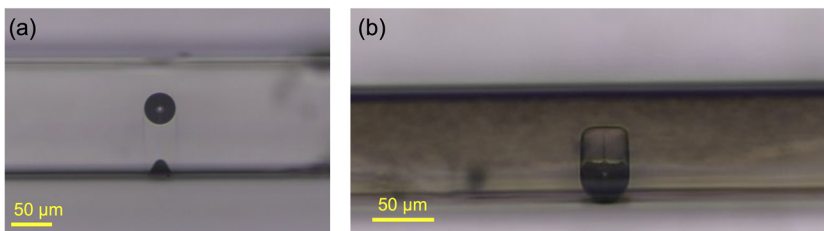

(a) 50 μm

(b) 50 μm

FIG. 7. Optical microscopy images showing the effects of shadowing from the microsphere over the SU-8 cross-link. (a) shadowing is mitigated by spinning the thicker layer first and (b) when the microsphere is closer to the substrate, the region beneath it is not cross-linked and the sphere sinks to the bottom.

the designated thicknesses and the use of specifically designed photolithography masks to ensure placement of the void at a desired location within the target. Imaging and absorption data confirm the viability of this approach and the reproducibility of the results over hundreds of targets. Furthermore, production of up to 50–60 targets can be achieved within a single fabrication procedure, ensuring high uniformity over several tens of devices. Scalability and high reproducibility make this technique suited for future studies at a high repetition rate, and the fabrication details can also be optimized for different experimental scopes, e.g., using metal-coated or filled spheres for viscosity measurements.

ACKNOWLEDGMENTS

AUTHOR DECLARATIONS

Conflict of Interest

The authors have no conflicts to disclose.

Author Contributions

Silvia Pandolfi: Conceptualization (lead); Methodology (lead); Writing – original draft (lead). **Thomas Carver**: Conceptualization (equal); Methodology (equal); Writing – review & editing(equal). **Daniel Hodge**: Data curation (equal); Writing – review & editing (equal). **Andrew F. T. Leong**: Writing – review & editing (equal). **Kelin Kurzer-Ogul**: Writing – review & editing (equal). **Philip Hart**: Data curation (equal). **Eric Galtier**: Data curation (equal). **Dimitri Khaghani**: Data curation (equal). **Eric Cunningham**: Data curation (equal). **Bob Nagler**: Data curation (equal). **Hae Ja Lee**: Data curation (equal). **Cindy Bolme**: Conceptualization (equal); Writing – review & editing (equal). **Kyle Ramos**: Conceptualization (equal); Writing – review & editing (equal). **Kenan Li**: Writing – review & editing (equal). **Yanwei Liu**: Writing – review & editing (equal). **Anne Sakdinawat**: Writing – review & editing (equal). **Stefano Marchesini**: Writing – review & editing (equal). **Pawel M. Kozlowski**: Writing – review & editing (equal). **Chandra B. Curry**: Writing – review & editing (equal). **Franz-Joseph Decker**: Writing – review & editing (equal). **Sharon Vetter**: Writing – review & editing (equal). **Jessica Shang**: Writing – review & editing (equal). **Hussein Aluie**: Writing – review & editing (equal). **Matthew Dayton**: Writing – review & editing (equal). **David S. Montgomery**: Conceptualization (equal); Writing – review & editing (equal). **Richard L. Sandberg**: Conceptualization (equal); Writing – review & editing (equal). **Arianna E. Gleason**: Conceptualization (equal); Data curation (equal); Funding acquisition (equal); Methodology (equal); Writing – original draft (equal).

DATA AVAILABILITY

The data that support the findings of this study are available from the corresponding author upon reasonable request.

REFERENCES

[1]D. B. Larson and G. D. Anderson, J. Geophys. Res.: Solid Earth **84**, 4592, https://doi.org/10.1029/jb084ib09p04592 (1979).

[2]R. A. Sacks and D. H. Darling, Nucl. Fusion **27**, 447 (1987).

[3]R. E. Olson, M. J. Schmitt, B. M. Haines, G. E. Kemp, C. B. Yeamans, B. E. Blue, D. W. Schmidt, A. Haid, M. Farrell, P. A. Bradley, H. F. Robey, and R. J. Leeper, Phys. Plasmas **28**, 122704 (2021).

[4]Y. T. Nguyen, D. Perera, P. Zhao, T. Sewell, and H. S. Udaykumar, Propellants, Explos., Pyrotech. **47**, e202200016 (2022).

[5]Z. Ding and S. M. Gracewski, J. Fluid Mech. **309**, 183 (1996).

[6]N. A. Hawker and Y. Ventikos, J. Fluid Mech. **701**, 59 (2012).

[7]J. H. J. Niederhaus, J. A. Greenough, J. G. Oakley, D. Ranjan, M. H. Anderson, and R. Bonazza, J. Fluid Mech. **594**, 85 (2007).

[8]D. Ranjan, M. Anderson, J. Oakley, and R. Bonazza, Phys. Rev. Lett. **94**, 184507 (2005).

[9]D. Ranjan, J. Oakley, and R. Bonazza, Fluid Mech. **43**, 117 (2011).

[10]S. J. Ali, P. M. Celliers, S. Haan, T. R. Boehly, N. Whiting, S. H. Baxamusa, H. Reynolds, M. A. Johnson, J. D. Hughes, B. Watson, H. Huang, J. Biener, K. Engelhorn, V. A. Smalyuk, and O. L. Landen, Phys. Plasmas **25**, 092708 (2018).

[11]R. Betti and O. A. Hurricane, Nat. Phys. **12**, 435 (2016).

[12]R. S. Craxton, K. S. Anderson, T. R. Boehly, V. N. Goncharov, D. R. Harding, J. P. Knauer, R. L. McCrory, P. W. McKenty, D. D. Meyerhofer, J. F. Myatt, A. J. Schmitt, J. D. Sethian, R. W. Short, S. Skupsky, W. Theobald, W. L. Kruer, K. Tanaka, R. Betti, T. J. B. Collins, J. A. Delettrez, S. X. Hu, J. A. Marozas, A. V. Maximov, D. T. Michel, P. B. Radha, S. P. Regan, T. C. Sangster, W. Seka, A. A. Solodov, J. M. Soures, C. Stoeckl, and J. D. Zuegel, Phys. Plasmas **22**, 110501 (2015).

[13]V. T. Tikhonchuk, Philos. Trans. R. Soc. **378**, 20200013 (2020).

[14]D. Sc, Fusion Energy Sciences Advisory Committee Long Range Planning Report, Powering the Future: Fusion & Plasmas, 2021.

[15]A. L. Kritcher, A. B. Zylstra, D. A. Callahan, O. A. Hurricane, C. Weber, J. Ralph, D. T. Casey, A. Pak, K. Baker, B. Bachmann, S. Bhandarkar, J. Biener, R. Bionta, T. Braun, M. Bruhn, C. Choate, D. Clark, J. M. Di Nicola, L. Divol, T. Doeppner,

V. Geppert-Kleinrath, S. Haan, J. Heebner, V. Hernandez, D. Hinkel, M. Hohenberger, H. Huang, C. Kong, S. Le Pape, D. Mariscal, E. Marley, L. Masse, K. D. Meaney, M. Millot, A. Moore, K. Newman, A. Nikroo, P. Patel, L. Pelz, N. Rice, H. Robey, J. S. Ross, M. Rubery, J. Salmonson, D. Schlossberg, S. Sepke, K. Sequoia, M. Stadermann, D. Strozzi, R. Tommasini, P. Volegov, C. Wild, S. Yang, C. Young, M. J. Edwards, O. Landen, R. Town, and M. Herrmann, Phys. Plasmas **28**, 072706 (2021).

[16]A. B. Zylstra, O. A. Hurricane, D. A. Callahan, A. L. Kritcher, J. E. Ralph, H. F. Robey, J. S. Ross, C. V. Young, K. L. Baker, D. T. Casey, T. Döppner, L. Divol, M. Hohenberger, S. Le Pape, A. Pak, P. K. Patel, R. Tommasini, S. J. Ali, P. A. Amendt, L. J. Atherton, B. Bachmann, D. Bailey, L. R. Benedetti, L. B. Hopkins, R. Betti, S. D. Bhandarkar, J. Biener, R. M. Bionta, N. W. Birge, E. J. Bond, D. K. Bradley, T. Braun, T. M. Briggs, M. W. Bruhn, P. M. Celliers, B. Chang, T. Chapman, H. Chen, C. Choate, A. R. Christopherson, D. S. Clark, J. W. Crippen, E. L. Dewald, T. R. Dittrich, M. J. Edwards, W. A. Farmer, J. E. Field, D. Fittinghoff, J. Frenje, J. Gaffney, M. G. Johnson, S. H. Glenzer, G. P. Grim, S. Haan, K. D. Hahn, G. N. Hall, B. A. Hammel, J. Harte, E. Hartouni, J. E. Heebner, V. J. Hernandez, H. Herrmann, M. C. Herrmann, D. E. Hinkel, D. D. Ho, J. P. Holder, W. W. Hsing, H. Huang, K. D. Humbird, L. Izumi, L. C. Jarrott, I. Jeet, O. Jones, G. D. Kerbel, S. M. Kerr, S. F. Khan, J. Kilkenny, Y. Kim, H. G. Kleinrath, V. G. Kleinrath, C. Kong, J. M. Koning, J. J. Kroll, M. K. G. Kruse, B. Kustowski, O. L. Landen, S. Langer, D. Larson, N. C. Lemos, J. D. Lindl, T. Ma, M. J. MacDonald, B. J. MacGowan, A. J. Mackinnon, S. A. MacLaren, A. G. MacPhee, M. M. Marinak, D. A. Mariscal, E. V. Marley, L. Masse, K. Meaney, N. B. Meezan, P. A. Michel, M. Millot, J. L. Milovich, J. D. Moody, A. S. Moore, J. W. Morton, T. Murphy, K. Newman, J.-M. G. Di Nicola, A. Nikroo, R. Nora, M. V. Patel, L. J. Pelz, J. L. Peterson, Y. Ping, B. B. Pollock, M. Ratledge, N. G. Rice, H. Rinderknecht, M. Rosen, M. S. Rubery, J. D. Salmonson, J. Sater, S. Schiaffino, D. J. Schlossberg, M. B. Schneider, C. R. Schroeder, H. A. Scott, S. M. Sepke, K. Sequoia, M. W. Sherlock, S. Shin, V. A. Smalyuk, B. K. Spears, P. T. Springer, M. Stadermann, S. Stoupin, D. J. Strozzi, L. J. Suter, C. A. Thomas, R. P. J. Town, E. R. Tubman, P. L. Volegov, C. R. Weber, K. Widmann, C. Wild, C. H. Wilde, B. M. V. Wonterghem, D. T. Woods, B. N. Woodworth, M. Yamaguchi, S. T. Yang, and G. B. Zimmerman, Nature **601**, 542 (2022).

[17]V. A. Smalyuk, C. R. Weber, O. L. Landen, S. Ali, B. Bachmann, P. M. Celliers, E. Dewald, A. Fernandez, B. A. Hammel, G. Hall, A. G. MacPhee, L. Pickworth, H. F. Robey, N. Alfonso, K. L. Baker, L. F. B. Hopkins, L. Carlson, D. T. Casey, D. S. Clark, J. Crippen, L. Divol, T. Döppner, J. Edwards, M. Farrell, S. Felker, J. E. Field, S. W. Haan, A. V. Hamza, M. Havre, M. C. Herrmann, W. W. Hsing, S. Khan, J. Kline, J. J. Kroll, S. LePape, E. Loomis, B. J. MacGowan, D. Martinez, L. Masse, M. Mauldin, J. L. Milovich, A. S. Moore, A. Nikroo, A. Pak, P. K. Patel, J. L. Peterson, K. Raman, B. A. Remington, N. Rice, M. Schoff, M. Stadermann, and S. A. Yi, High Energy Density Phys. **36**, 100820 (2020).

[18]R. E. Kidder, Nucl. Fusion **16**, 3 (1976).

[19]L. Soulard, N. Pineau, J. Clérouin, and L. Colombet, J. Appl. Phys. **117**, 115901 (2015).

[20]J. D. Kilkenny, S. G. Glendinning, S. W. Haan, B. A. Hammel, J. D. Lindl, D. Munro, B. A. Remington, S. V. Weber, J. P. Knauer, and C. P. Verdon, Phys. Plasmas **1**, 1379 (1994).

[21]S. X. Hu, V. N. Goncharov, P. B. Radha, S. P. Regan, and E. M. Campbell, Nucl. Fusion **59**, 032011 (2018).

[22]R. F. Smith, V. Rastogi, A. E. Lazicki, M. G. Gorman, R. Briggs, A. L. Coleman, C. Davis, S. Singh, D. McGonegle, S. M. Clarke, T. Volz, T. Hutchinson, C. McGuire, D. E. Fratanduono, D. C. Swift, E. Folsom, C. A. Bolme, A. E. Gleason, F. Coppari, H. J. Lee, B. Nagler, E. Cunningham, P. Heimann, R. G. Kraus, R. E. Rudd, T. S. Duffy, J. H. Eggert, and J. K. Wicks, J. Appl. Phys. **131**, 245901 (2022).

[23]L. Altshuler, G. Doronin, and G. Kh. Kim, Appl. Mech. Tech. Phys. **110**, 887–894 (1987).

[24]G. Kh. Kim, J. Appl. Mech. Tech. Phys. **25**, 692–695 (1984).

[25]D. B. Bober, J. Lind, and M. Kumar, Phys. Rev. Mater. **3**, 073603 (2019).

[26]FESAC, Powering the Future - Fusion & Plasmas, 2020.

[27]S. W. Haan, H. Huang, M. A. Johnson, M. Stadermann, S. Baxamusa, S. Bhandarkar, D. S. Clark, V. Smalyuk, and H. F. Robey, Phys. Plasmas **22**, 032708 (2015).

[28]S. Haan et al., "Comparison of the three NIF ablators," Internal Report No. LLNL-TR-741418, 2017.

[29]B. Cook et al., "Preliminary evaluation of techniques to fabricate beryllium, polyimide, and Ge- doped CH/CD ablator materials," LLNL Internal Report No. UCRL-TR-208476, 2004.

[30]S. J. Ali, P. M. Celliers, S. W. Haan, T. R. Boehly, N. Whiting, S. H. Baxamusa, H. Reynolds, M. A. Johnson, J. D. Hughes, B. Watson, K. Engelhorn, V. A. Smalyuk, and O. L. Landen, Phys. Rev. E **98**, 033204 (2018).

[31]J. M. Shaw, J. D. Gelorme, N. C. LaBianca, W. E. Conley, and S. J. Holmes, IBM J. Res. Dev. **41**, 81 (1997).

[32]J. Orava, T. Kohoutek, and T. Wagner, *Part Prep. Prop. Chalcogenide Glasses* (Science Direct, 2014), Chap. 9 p. 265.

[33]Z.-F. Zhou and Q.-A. Huang, Micromachines **9**, 341 (2018).

[34]I. Roch, P. Bidaud, D. Collard, and L. Buchaillot, J. Micromech. Microeng. **13**, 330 (2003).

[35]T. Xu, J. H. Yoo, S. Babu, S. Roy, J.-B. Lee, and H. Lu, J. Micromech. Microeng. **26**, 105001 (2016).

[36]T. C. Sum, A. A. Bettiol, J. A. van Kan, F. Watt, E. Y. B. Pun, and K. K. Tung, Appl. Phys. Lett. **83**, 1707 (2003).

[37]S. A. Saq'an, A. S. Ayesh, A. M. Zihlif, E. Martuscelli, and G. Ragosta, Polym. Test. **23**, 739 (2004).

[38]K.-Y. Hung and T.-H. Liang, Microsyst. Technol. **14**, 1217 (2008).

[39]A. del Campo and C. Greiner, J. Micromech. Microeng. **17**, R81 (2007).

[40]J. Liu, B. Cai, J. Zhu, G. Ding, X. Zhao, C. Yang, and D. Chen, Microsyst. Technol. **10**, 265 (2004).

[41]D. H. Dolan, Sandia Report SAND2006-1950, 2006.

[42]S. B. Brown, A. E. Gleason, E. Galtier, A. Higginbotham, B. Arnold, A. Fry, E. Granados, A. Hashim, C. G. Schroer, A. Schropp, F. Seiboth, F. Tavella, Z. Xing, W. Mao, H. J. Lee, and B. Nagler, Sci. Adv. **5**, eaau8044 (2019).

[43]R. L. Sandberg, C. Bolme, K. Ramos, Q. McCulloch, R. Martinez, V. Hamilton, T. Pierce, M. Greenfield, K. Brown, S. McGrane, J. L. Barber, B. Abbey, A. Schropp, F. Seiboth, P. Heiman, B. Nagler, E. Galtier, and E. Granados, *International Conference on Ultrafast Phenomena UTh4A* (Optica Publishing Group, 2016), p. 36.

[44]A. Schropp, R. Hoppe, V. Meier, J. Patommel, F. Seiboth, Y. Ping, D. G. Hicks, M. A. Beckwith, G. W. Collins, A. Higginbotham, J. S. Wark, H. J. Lee, B. Nagler, E. C. Galtier, B. Arnold, U. Zastrau, J. B. Hastings, and C. G. Schroer, Sci. Rep. **5**, 11089 (2015).

[45]R. L. Sandberg, C. Bolme, K. Ramos, Q. McCulloch, R. Martinez, V. Hamilton, T. Pierce, M. Greenfield, S. McGrane, J. L. Barber, B. Abbey, A. Schropp, F. Seiboth, P. Heiman, B. Nagler, E. Galtier, and E. Granados, Microsc. Microanal. **21**, 1851 (2015).

[46]B. Nagler, A. Schropp, E. C. Galtier, B. Arnold, S. B. Brown, A. Fry, A. Gleason, E. Granados, A. Hashim, J. B. Hastings, D. Samberg, F. Seiboth, F. Tavella, Z. Xing, H. J. Lee, and C. G. Schroer, Rev. Sci. Instrum. **87**, 103701 (2016).

[47]P. J. Withers, C. Bouman, S. Carmignato, V. Cnudde, D. Grimaldi, C. K. Hagen, E. Maire, M. Manley, A. Du Plessis, and S. R. Stock, Nat. Rev. Methods Primers **1**, 18 (2021).